Higher Frequency Modeling of Synchronous Exciter Machines by Equivalent Circuits and Transfer Functions

Marcus Banda

Abstract—In this article the influence of higher frequency effects in addition to a special damper design on the electrical behavior of a synchronous generator main exciter machine is investigated. On the one hand these machines are often highly stressed by harmonics from the bridge rectifier thus facing additional eddy current losses. On the other hand the switching may cause the excitation of dangerous voltage peaks in resonant circuits formed by the diodes of the rectifier and the commutation reactance of the machine. Therefore modern rotating exciters are treated like synchronous generators usually modeled with a second order equivalent circuit. Hence the well known Standstill Frequency Response Test (SSFR) method is applied to a test machine in order to determine parameters for the simulation. With these results it is clearly shown that higher frequencies have a strong impact on the conventional equivalent circuit model. Because of increasing field displacement effects in the stranded armature winding the sub-transient reactance is even smaller than the armature leakage at high frequencies. As a matter of fact this prevents the algorithm to find an equivalent scheme. This issue is finally solved using Laplace transfer functions fully describing the transient behavior at the model ports.

Keywords—Synchronous exciter machine, Linear transfer function, SSFR, Equivalent Circuit

I. INTRODUCTION

ROTATING brushless exciters are well established in providing the field current for synchronous generators. The advantages against slip rings with a stationary rectifier are the self-excitation by an auxiliary exciter and the low maintenance effort. The exciter system itself consists of a voltage regulator, a main and an auxiliary exciter machine and a rotating bridge rectifier. The aim of this paper is the detailed analysis of the main exciter machine as part of the whole exciter system. The examined machine type has a three phase armature winding in the laminated rotor, a concentrated salient-pole field winding in the laminated stator and no explicit damper winding. The function of a damper is provided by the stator steel lamination where eddy currents occur. Its sheets are thicker compared to the armature sheets and non-insulated against each other. This damper treatment can be derived from a massive pole shoe. Several authors [1] - [4] proposed exciter models and simulated the operating behavior.

In [1] a standard second order model was used to determine stresses of the several components in the power system, where the parameters were used from advanced calculation. But even in the stationary operation of the generator the exciter machine is always stressed by voltage and current harmonics in the rotor and in the stator winding due to the feedback from the bridge rectifier. In addition to that the switching cause the excitation of high frequent voltage peaks in resonant circuits formed from the capacitance of the diodes and the commutation reaction of the machine. This reactance is mainly calculated from the sub-transient values of the d- and q-axis. Accordingly the frequency range of conventional synchronous generator models is extended by orders. Beside the advanced calculation, extended efforts were made to measure the parameters at standstill. Actually two standards [5] and [6] provide a good base for the SSFR method. Apart from other authors dealing with these tests [7] - [9] focused on the low frequency generator application this article also concentrates on the high frequency behavior at several kHz.

II. DETERMINATION OF THE FREQUENCY BAHAVIOR

A. Application of the SSFR method

The conditions for the measurement are derived from the idea of two individual axis with no cross coupling flux effects during standstill in Fig. 1. The tests were carried out as shown in Fig. 2 with currents of about 1% of the nominal current.
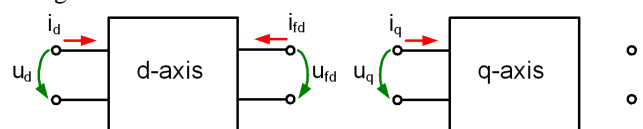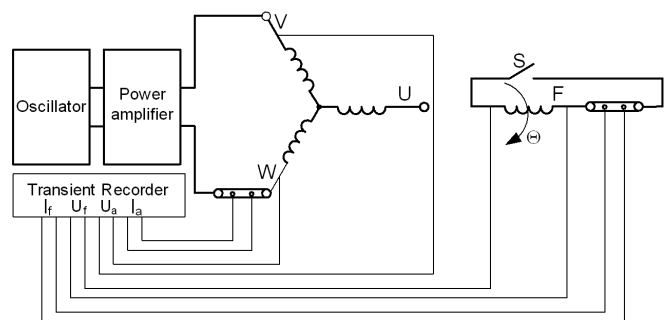

Fig. 1 Two-port network equivalent circuits

Fig. 2 Measurement scheme, S: Switch to shorten the field winding, Θ: angle of alignment between field and armature winding

Marcus Banda is with the Siemens AG, Energy Sector, Generator Plant Erfurt, Werner – von – Siemens Straße 1, 99086, Erfurt, Germany, (phone: +49(0)361-753-2548, fax: +49(0)361-753-2520, email:marcus.banda@siemens.com).

World Academy of Science, Engineering and Technology
International Journal of Electronics and Communication Engineering
Vol:6, No:3, 2012

As a first step the armature winding is fed by two phases connected in series. At the same time the rotor is shorted and turned until the maximum current is observed in the field winding. Thus both magnetic axis are aligned. In that position the input impedance of the d-axis $\underline{z}_d$ and the current transfer function G_{fd} are measured [5]:

$$\underline{z}_d = 1/2 \cdot \underline{u}_a / \underline{i}_a = \underline{u}_d / \underline{i}_d \mid u_{fd} = 0 \quad (1)$$

$$-p \cdot G_{fd} = \sqrt{3}/2 \cdot \underline{i}_{fd} / \underline{i}_a = \underline{i}_{fd} / \underline{i}_d \mid u_{fd} = 0 \quad (2)$$

The reactance operator x_d results from the impedance $\underline{z}_d$:

$$x_d(jv) = \left(\underline{z}_d(jv) - r_a \right)/jv \quad (3)$$

As a third relation the transfer impedance is found by leaving the field winding open and measure the induced voltage:

$$\underline{z}_{af0} = \sqrt{3}/2 \cdot \underline{u}_{fd} / \underline{i}_a = \underline{u}_{fd} / \underline{i}_d \mid i_{fd} = 0 \quad (4)$$

The last step is a re-alignment of the rotor into the quadrature axis by finding the minimum field current.

$$\underline{z}_q = 1/2 \cdot \underline{u}_a / \underline{i}_a = \underline{u}_q / \underline{i}_q \quad (5)$$

The reactance operator again results from the impedance $\underline{z}_q$:

$$x_q(jv) = \left(z_q(jv) - r_a \right)/jv \quad (6)$$

The measurement covered a wide frequency range from 1mHz to 10kHz.

B. Model Parameter Identification

Having determined the amplitudes and phase shifts of the sinusoidal voltages and currents at the ports, the four transfer functions $x_d(p)$, $x_q(p)$, $G_{fd}(p)$, $z_{af0}(p)$ are known at the measured points. In order to get a continuous relation between the input and output quantities linear transfer functions (LTF) of n-th order are used as an approach. The next equation starts exemplary with the complex admittance operators for the q-axis which is the same for the direct axis.

$$\frac{1}{x_q(j\omega)} = \frac{1}{x_q} + \left(\frac{1}{x_q'} - \frac{1}{x_q} \right) \cdot \frac{j\omega \cdot T_q'}{1 + j\omega \cdot T_q'} +$$
$$\dots + \left(\frac{1}{x_q^{(n)}} - \frac{1}{x_q^{(n-1)}} \right) \cdot \frac{j\omega \cdot T_q^{(n)}}{1 + j\omega \cdot T_q^{(n)}} \quad (7)$$

The parameter determination of these functions from the measurement ends up in a complex Least Square minimization problem. With the help of conventional mathematic tools the transfer functions are best fitted by applying either the Newton Raphson or Levenberg-Marquardt algorithm.

$$Q_{LS} = \sum_i \left| 1/x_{meas,i} - 1/x_{mod,i} \right|^2 \to \min! \quad (8)$$

Solving the least square (LS) equations for the whole frequency range the results are stated in Fig. 3, Fig. 4 and in Tables I and II. The higher the order of the fitting function is the smaller its remaining least square error becomes. Especially the second order fit for the quadrature axis leads to unacceptable discrepancies in the medium frequency range. The third order approximation is found to be reasonable. From the low frequency limits the 0Hz values are extrapolated to:

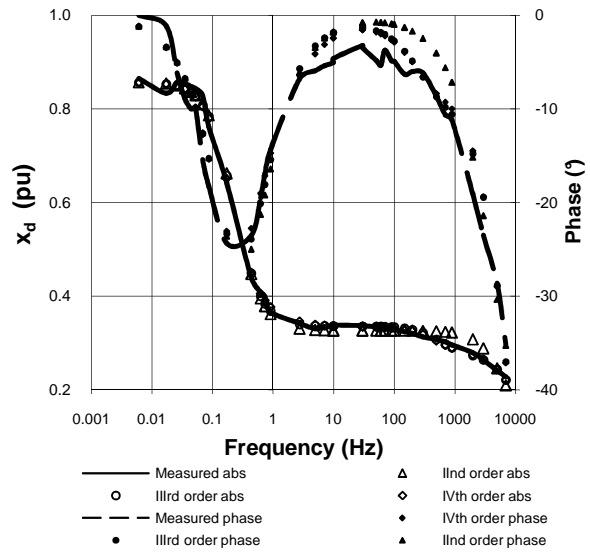$$x_{d0} = 0.865\,pu, \; x_{q0} = 0.680\,pu, \; r_a = 0.01\,pu$$
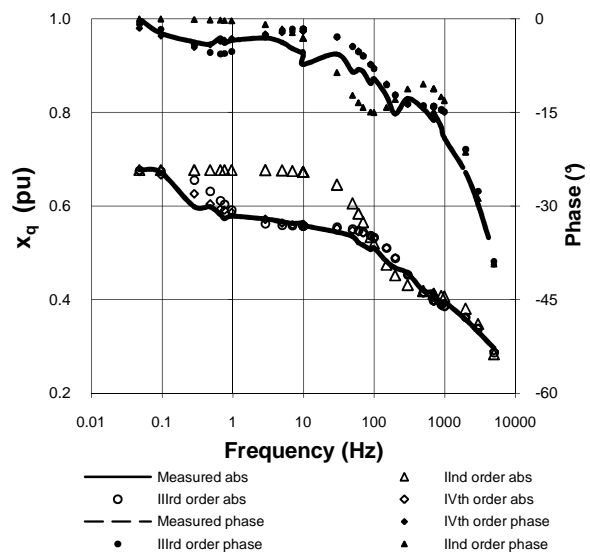

Fig. 3 Direct axis reactance transfer function

Fig. 4 Quadrature axis reactance transfer function

TABLE I
D-AXIS REACTANCE AND TIME CONSTANTS, 1E-3 TO 10E3 HZ

Symbol	IInd order	IIIrd order	IVth order
x_d'	0.326	0.336	0.351
x_d''	0.077	0.278	0.334
x_d'''	-	3.216m	0.281
x_d''''	-	-	7.946m
T_d'	0.333	0.353	0.383
T_d''	6.953u	254.8u	0.049
T_d'''	-	197.5n	292.7u
T_d''''	-	-	501.7n
$Error$	1.496	0.518	0.471

World Academy of Science, Engineering and Technology
International Journal of Electronics and Communication Engineering
Vol:6, No:3, 2012

TABLE II
Q- AXIS REACTANCE AND TIME CONSTANTS, 1E-3 TO 10E3 HZ

Symbol	IInd order	IIIrd order	IVth order
x'_q	0.418	0.558	0.582
x''_q	0.058	0.388	0.554
x'''_q	-	0.028	0.385
x''''_q	-	-	0.015
T'_q	1.34m	0.226	0.528
T''_q	4.861u	477.2u	0.042
T'''_q	-	2.105u	454.2
T''''_q	-	-	1.04u
$Error$	1.753	0.458	0.383

C. Equivalent Circuit Model

In the literature [8], [11] the way from the reactances and time constants determined in B to an easy to implement equivalent circuit is described thoroughly. The only required quantity to calculate in advance is the armature leakage reactance $x_{a\sigma} = 0.177$. This leakage reactance is either analytically calculated or by means of a detailed magnetic equivalent circuit as described in [10]. With the knowledge of the armature leakage and main field reactance the ladder network for the damper and the field winding is obtained by the separation from the frequency response. This approach is exemplified for the q-axis in appendix D. For the equivalent circuit models as shown in Fig. 5 and Fig. 6 it is obligatory to have the highest order reactance smaller than the previously introduced armature leakage reactance.
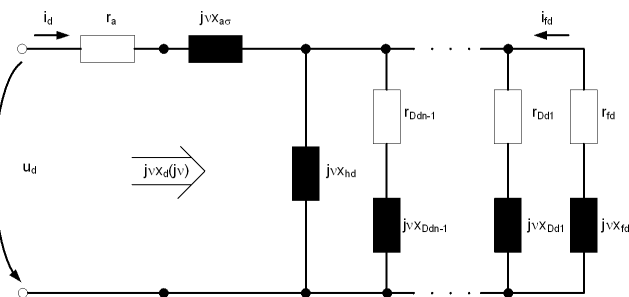
$$x^{(n)} > x_{a\sigma} \qquad (9)$$

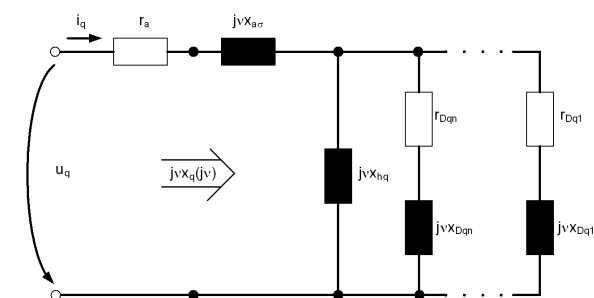Fig. 5 Equivalent circuit for the direct axis during standstill u$_{fd}$=0

Fig. 6 Equivalent circuit for the quadrature axis during standstill u$_{fd}$=0

This condition is neither kept for the d-axis nor for the q-axis. The reason for that is the increasing field displacement at higher frequencies taking effect in the armature slots on the stranded winding. In contrast to standard synchronous machines for generator application this high frequency effect is mostly not considered because the recommended upper frequency limit for the measurement is three times the rated frequency (150-180Hz). In order to keep the conventional model structure the fitting process is cut off at a frequency of about 1kHz. Nevertheless the results are still in a good agreement till the middle of this order of magnitude. With this limitation the following results were achieved:

TABLE III
D-AXIS REACTANCE AND TIME CONSTANTS, 1E-3 TO 1E3 HZ

Symbol	IInd order	IIIrd order	IVth order
x'_d	0.334	0.342	0.354
x''_d	0.223	0.314	0.337
x'''_d	-	0.179	0.313
x''''_d	-	-	0.179
T'_d	0.349	0.366	0.393
T''_d	122.6u	1.709m	0.045
T'''_d	-	54.84u	1.35m
T''''_d	-	-	54.42u
$Error$	0.394	0.197	0.177

TABLE IV
Q- AXIS REACTANCE AND TIME CONSTANTS, 1E-3 TO 1E3 HZ

Symbol	IInd order	IIIrd order	IVth order
x'_q	0.548	0.571	0.588
x''_q	0.308	0.445	0.547
x'''_q	-	0.209	0.433
x''''_q	-	-	0.179
T'_q	0.324	0.492	0.65
T''_q	188.6u	1.301m	0.016
T'''_q	-	54.67u	941.5u
T''''_q	-	-	39.43u
$Error$	0.67	0.181	0.131

Alternatively a ladder network for the armature leakage as mentioned in [15] might be used. From these tables it becomes obvious that even the highest order reactance is greater than the armature leakage. The values for the equivalent schemes from Fig. 5 and Fig. 6 can be derived accordingly. But still only two reactance operator functions out of four transfer functions were taken into account. As a matter of fact the current transfer function as shown in Fig. 7 yields only a good agreement till frequencies of 100Hz. At higher frequencies the correlation to the measurement becomes even worse due to the wrong flux distribution between the damper and the field winding which is already described in the literature [8], [12]. Consequently the models for the direct axis have to take this current transfer function into consideration without falsifying the input impedance. For the second and the third order model

World Academy of Science, Engineering and Technology
International Journal of Electronics and Communication Engineering
Vol:6, No:3, 2012

the amplitude and respectively the phase shift of $p \cdot G_{fd}$ are considered in the parameter determination process ending up with the characteristic reactance as pointed out in Fig. 8.
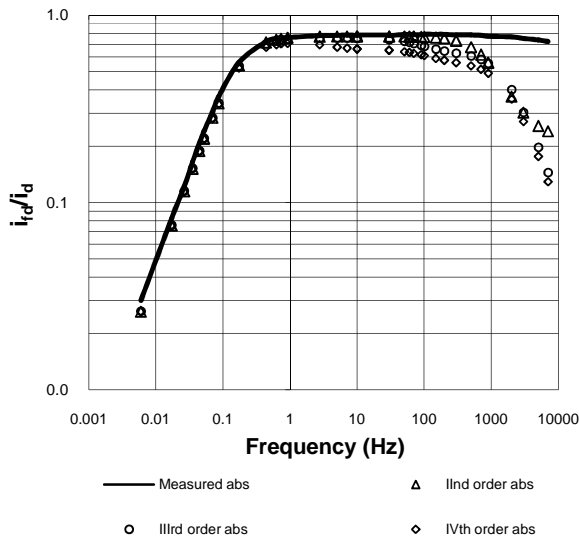

Fig. 7 Field to armature current transfer function

The following tables state the resulting equivalent circuit values for the direct axis with and without the characteristic reactance. Actually there is no such value for the quadrature axis.

TABLE V
D-AXIS EQUIVALENT CIRCUIT MODEL PARAMETERS, 1E-3 TO 1E3 HZ

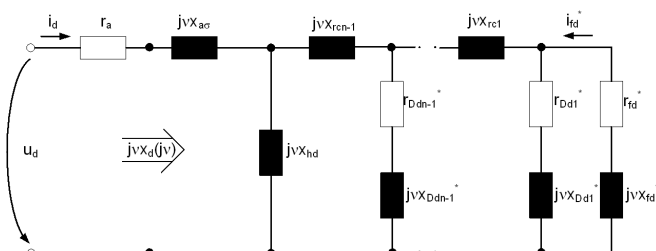| Symbol	IInd order	IIIrd order	IVth order
r_{fd}	$786.4u / 723.4u$	$780u / 705.9u$	$780u$
x_{fd}	$0.204 / 0.726$	$0.218 / 1.799$	0.245
x_{rc1}	$- / - 0.532$	$- / - 1.371$	-
x_{rc2}	-	$- / - 0.228$	-
r_{Dd1}	$0.956 / 13.732$	$0.439 / 40.235$	0.027
x_{Dd1}	$0.064 / 2.886$	$0.855 / 66.656$	1.463
r_{Dd2}	-	$1.149 / 7.139$	0.612
x_{Dd2}	-	$1.795m / 0.515$	0.951
r_{Dd3}	-	-	1.153
x_{Dd3}	-	-	$1.795m$

Fig. 8 Equivalent circuit for the direct axis considering the common leakage

TABLE VI
Q-AXIS EQUIVALENT CIRCUIT MODEL PARAMETERS, 1E-3 TO 1E3 HZ

Symbol	IInd order	IIIrd order	IVth order
r_{Dq1}	0.00385	0.00320	0.00300
x_{Dq1}	1.438	1.851	2.314
r_{Dq2}	1.363	0.630	0.187
x_{Dq2}	0.203	0.904	3.742
r_{Dq3}	-	2.084	0.878
x_{Dq3}	-	0.036	0.913
r_{Dq4}	-	-	2.162
x_{Dq4}	-	-	0.001784

D. Transfer function model

The equivalent circuit approach was historically chosen to speed up the simulation. Nowadays the simulation of linear transfer functions (LTF) is well established. Many circuit simulators are able to include Laplace transfer functions in their modeling code. Therefore, the transient analysis of the complete system consisting of generator, grid and excitation can be combined with transfer functions. Contrary to simple LTF models for a regulator [14] the implementation into a simulation background leads to the problem of conservative electric nodes which need to have the coincidental formulation because of the unknown energy flow direction. The main difference compared to the equivalent circuit modeling is the unimportance of the physical flux location. Only the electrical behavior at the machine ports is of interest. Following the formulas in [13] the differential system of equations is transferred by Laplace transform. The Normalization of the quantities strictly follows the literature. But time is not normalized to not complicate the simulation model. Beside the exciter it also includes the rectifier, the generator and the voltage regulator where pu-port quantities would be of disadvantage. Especially because the generator and the exciter have different reference angular velocities. Although the inner model is supposed to be in pu values the terminal quantities are supposed to give the real values as shown in Fig. 9. As a consequence, the additional factor ω_N will appear in the equations. By using the mere frequency transfer functions no limitation with regard to the frequency range is required.
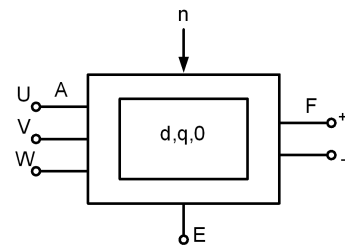

Fig. 9 Blackbox modeling of the machine, F: Field winding, A: Armature winding with phases U/V/W, E: Neutral/Ground connection, n: speed (coupled to generator), d/q/0: model quantities referred to armature winding and pole coordinate system

World Academy of Science, Engineering and Technology
International Journal of Electronics and Communication Engineering
Vol:6, No:3, 2012

The subsequent system of equations includes the four mandatory transfer functions to reproduce the measured system behaviors. The initial conditions are set to zero. This first set of equations yields a formulation for direct axis flux linkage and the field current:

$$\begin{pmatrix} \underline{\Psi}_d \\ \underline{i}_{fd} \end{pmatrix} = \begin{pmatrix} x_d(p) & G_{fd}(p) \cdot \omega_N \\ -p \cdot G_{fd}(p) & F_{fd}(p) \end{pmatrix} \cdot \begin{pmatrix} \underline{i}_d \\ \underline{u}_{fd} \end{pmatrix} \qquad (10)$$

with

$$F_{fd}(p) = p \cdot G_{fd}(p) / z_{af0}(p) \qquad (11)$$

The last equation shows the quadrature axis flux linkage.

$$\underline{\Psi}_q = x_q(p) \cdot \underline{i}_q \qquad (12)$$

The measured parameter values for the reactance operator functions $x_d(p)$ and $x_q(p)$ correspond with (7) and the values in Table I and II for the third order model. The last two transfer functions are found in accordance with the subsequent equations.

$$p \cdot G_{fd} = p \cdot 0.794s / (1 + p \cdot 1.032s) \qquad (13)$$

$$\underline{z}_{af0} = \frac{-p \cdot 542.2 \cdot 10^{-6}s}{(1 + p \cdot 815.5 \cdot 10^{-6}s)} \cdot \frac{(1 + p \cdot 240.8 \cdot 10^{-6}s)}{(1 + p \cdot 68.94 \cdot 10^{-6}s)} \qquad (14)$$

The set of equations for the full model description is supplemented by the voltage equations in appendix B.

III. COMPARISON OF THE TWO MODELS AND QUALITY OF FIT

For the upper frequency limit which is to take into consideration important frequencies need to be known. With the Turbine-Generator-Exciter machine train rotating at grid frequency f_{gr} of 50 or 60Hz and the machine having multiple pole pairs $n_{pp} = 4$ the resulting electrical frequency is $f_{el} = n_{pp} \cdot f_{gr} = 200 / 240 Hz$. Due to the bridge rectifier this frequency is multiplied by the characteristic factor of the rectifier which is six in the example. With the measurement presented it is obvious that the application of the conventional equivalent circuit structure might not be sufficient for modeling especially the commutation effects stressing the diodes and the resonances in the range of several kHz. Therefore the upper frequency limit was pushed far beyond the recommended frequency in [5] and the grid frequency of the synchronous generator. The application of the SSFR method revealed important information about the machine behavior especially confirming the efficiency of the damper construction. Although the stator is laminated eddy currents occur and filter out harmonics from the field winding. In addition to that the limits of the common equivalent circuit could be shown and the advantage of the LTF model was examined for the usage in a transient simulation. Next graphs summarize the results of the measurement extrapolated to 100kHz. The fourth order approximation was replaced by the LTF model in the graphs.
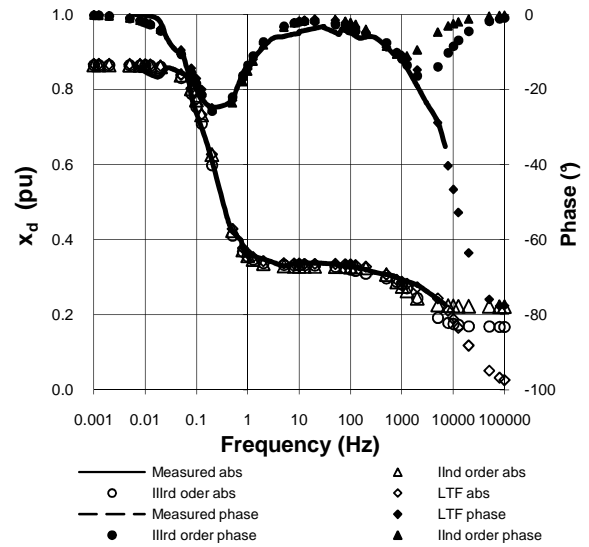

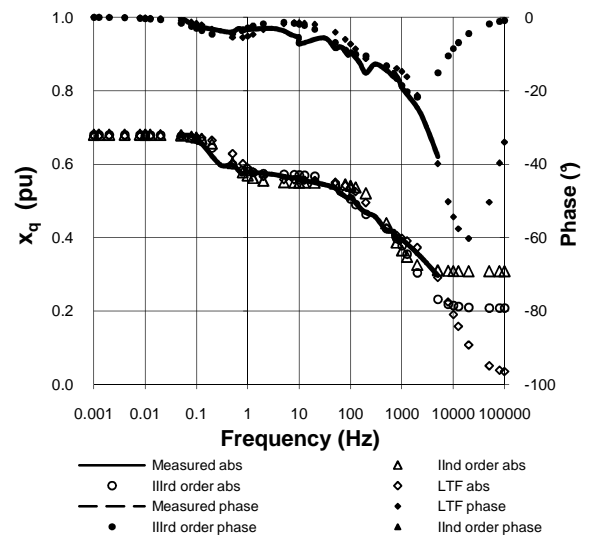Fig. 10 Reactance operator direct axis

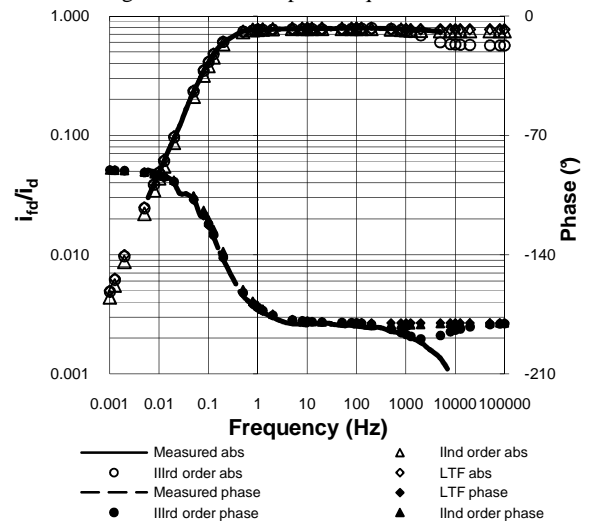Fig. 11 Reactance operator quadrature axis

Fig. 12 Current transfer function

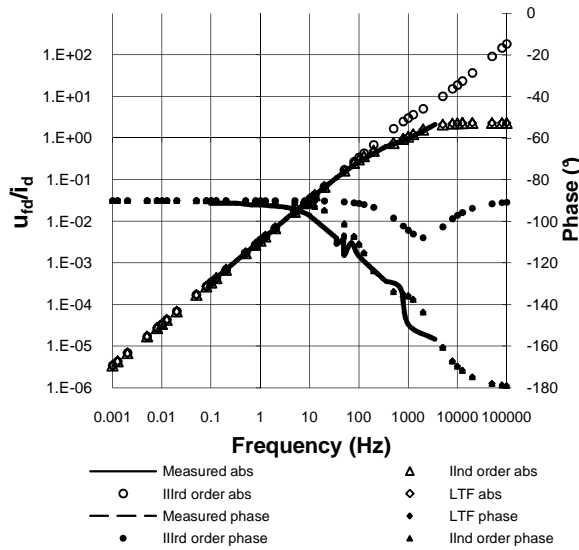World Academy of Science, Engineering and Technology
International Journal of Electronics and Communication Engineering
Vol:6, No:3, 2012

Fig. 13 Comparison of the Transfer impedances

APPENDIX

A. Nomenclature

Indices

0	Zero Sequence
a	Armature (winding)
d	Direct axis
D	Damper
f	Field (winding)
meas	measured
mod	model
q	Quadrature axis
σ	Leakage

Symbols

j	Complex number
n	Relative speed
p	Laplace variable, for zero damping $p \rightarrow j\omega$
r, x	Resistance in pu, Reactance in pu
T	Time constant in s
$\underline{z}$	Complex impedance
$v = \omega / \omega_N$	Relative frequency
ω	Angular frequency
ω_N	Nominal angular frequency

B. Voltage equations for the transfer function model

$$u_d = r \cdot i_d + p \cdot \left(\Psi_d - \Psi_{d,t=0} / p \right) / \omega_N - n \cdot \Psi_q \qquad (15)$$

$$u_q = r \cdot i_q + p \cdot \left(\Psi_q - \Psi_{q,t=0} / p \right) / \omega_N + n \cdot \Psi_d \qquad (16)$$

$$u_0 = r_0 \cdot i_0 + p \cdot x_0 \cdot \left(i_0 - i_{0,t=0} / p \right) / \omega_N \qquad (17)$$

C. Identification of the equivalent damper/field branches

In order to calculate the elements of the ladder network for the equivalent circuit the admittance is a sum of the parallel branches of the in series connected resistors and reactance:

$$\underline{Y}_{\|} = \sum_i 1 / \left(r_i + j v \cdot x_i \right) \qquad (18)$$

Using the input impedance based on the equivalent circuit in (19) the branch impedance is obtained in (20).

$$j v \cdot x_q (j v) = j v \cdot x_{a\sigma} + j v \cdot x_{hq} / \left(1 + j v \cdot x_{hq} \cdot \underline{Y}_{\|} \right) \qquad (19)$$

$$1 / \underline{Y}_{\|} = j v \cdot x_{hq} \cdot \left(x_q (j v) - x_{a\sigma} \right) / \left(x_{hq} + x_{a\sigma} - x_q (j v) \right) \qquad (20)$$

Resulting in the fraction (20) the constant parameters of the partial fraction elements are easily calculated by using the Heavy-side cover up method.

$$R / Q = \left(x_{hq} + x_{a\sigma} - x_q (j v) \right) / \left(j v \cdot x_{hq} \cdot \left(x_q (j v) - x_{a\sigma} \right) \right) = \sum_i A_i / \left(B_i + j v \right) \qquad (21)$$

Finally the reactance and the resistance of the ladder network are determined with (22) and (23).

REFERENCES

[1] D. R. Gomes, I.E. Chabu, "Studies on electrical stresses in rotating rectifiers for brushless exciters", IEEE/IAS Internal Conference of Industrial Applications, November 2010
[2] S.M.L. Kabir, R. Shuttleworth, "Brushless exciter models", IEE Proc.-Gener. Trans. Distrib., Vol. 141, No.1, January 1994
[3] M. Shahnazari, A. Vahedi, "Analysis of brushless exciter operation in all modes of rotating rectifiers", 4th IEEE Conference on Industrial Electronics and Applications, ICIEA 2009, June 2009
[4] M.A. Abdel-Halim, C.D. Manning, "Modeling a laminated brushless exciter-alternator unit in all modes of operation", IEE Proceedings-B, Vol.138, No.2, March 1991
[5] IEEE Std 115-1995, "Obtaining Synchronous Machine Parameters by Standstill Frequency Response Test"
[6] DIN EN 60034-4, 2009, "Verfahren zur Ermittlung von Kenngrößen von Synchronmaschinen durch Messung"
[7] P.L. Dandeno, A.T. Poray, "Development of detailled Turbogenerator equivalent circuits from standstill frequency response measurements", IEEE Transactions on Power Apparatus and Systems, Vol. PAS-100, No. 4, April 1981, Ontario Hydro
[8] I.M. Canay, "Determination of the model parameters of machines from the reactance operators $x_d(p)$, $x_q(p)$ (Evaluation of the Standstill Frequency Response Test)", IEEE Transactions on Energy Conversion, Vol.8, No.2, June 1993
[9] M. Freese, M. Klocke, "Aspects of Identification of equivalent circuit parameters of large synchronous generators by SSFR – Tests", Proceedings of XLIIIrd International Symposium on Electrical Machines SME 2007, 2 -5 July, Poznań, Poland
[10] M. Banda, O. Michelsson, "A new network calculation model for the predetermination of the exciter current and the reactance of salient-pole synchronous machine", Information Technology and Electrical Engineering - Devices and Systems, Materials and Technologies for the Future, IWK, Internationales Wissenschaftliches Kolloquium der TU Ilmenau, 54 / 2009 / 20100305890
[11] I.M. Canay, "Modeling of alternating-current machines having multiple rotor circuits", IEEE Transactions on Energy Conversion, Vol. 8, No.2 , June 1993
[12] I.M., Canay, "Causes of Discrepancies on calculation of rotor quantities and exact equivalent diagrams of the synchronous machine", IEEE Transactions on Power Apparatus and Systems, Vol. PAS-88, pp.1114-1120, July 1969
[13] Ponick, B., Müller, G., "Theorie elektrischer Maschinen", 6. Auflage, 2009, Wiley-VCH
[14] I. M. Canay, "Block Diagrams and Transfer Functions of the Synchronous Machine", IEEE TRANSACTIONS ON POWER APPARATUS AND SYSTEMS, VOL. PAS-85, No. 9, 1966
[15] K.H. Dempewolf, "Transiente Simulation eines Antriebssystems zur Bestimmung der frequenzabhängigen Verluste in schnelllaufenden permanenterregten Synchronmaschinen", Internationaler ETG Kongress Karlsruhe 2007